

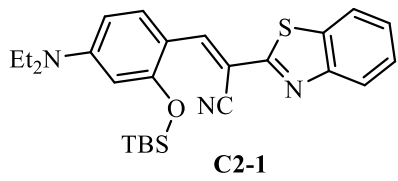
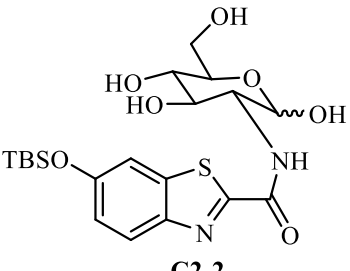
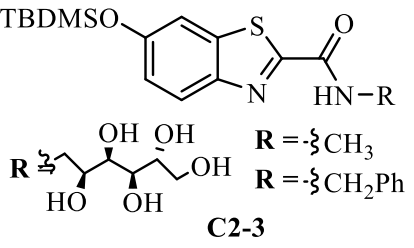
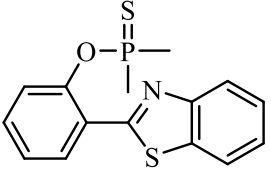
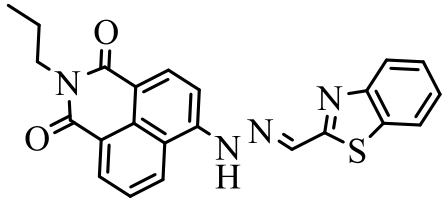
Chapter 2

Fluoride sensing study of benzothiazole based organic probe molecules having amine and amide moieties in aqueous medium

2.1. Introduction

The development of chemical sensors for detecting various ions is a significant area of research due to their applications in environmental monitoring, biological imaging, and industrial processes [1-3]. Benzothiazole-based fluorescent probes have proven to be highly effective because of their unique structural and photophysical properties [4]. Benzothiazole is a heterocyclic aromatic organic compound and an important pharmacophore, often regarded as a privileged structure in medicinal chemistry [5-8]. This bicyclic compound consists of the fusion of benzene and thiazole rings and is a moiety of choice due to its numerous pharmacological properties [9]. Notably, many compounds in nature, including vitamins like B1, contains heterocyclic rings with nitrogen and sulphur atoms [10]. These heterocycles are found in many pharmacologically and biologically active compounds. Benzothiazoles exhibit a range of medicinal properties, including anti-inflammatory [11], antimicrobial [12], anti-bacterial [13], anticancer [14], and anti-Alzheimer's effects [15], etc. Benzothiazole derivatives are particularly suitable for sensing cations due to their electron-rich structure, which facilitates strong electrostatic interactions resulting in noticeable changes in photophysical properties [16]. Additionally, benzothiazole can be easily functionalized to introduce specific binding sites for anions, enhancing selectivity and sensitivity. The stable conjugated systems in benzothiazole-based probes undergo significant electronic changes upon binding with anions, providing measurable colorimetric and fluorometric responses. Their excellent optical properties, including high absorptivity, quantum yields and good photostability, contribute to the clear and strong signals necessary for anion detection [17]. Furthermore, benzothiazole derivatives are biocompatible and exhibit low toxicity, making them suitable for biological applications such as live-cell imaging and in vivo studies. The robustness and versatility of benzothiazole's conjugated system allow for better signal transduction and stability in aqueous medium. The high selectivity and sensitivity of benzothiazole-based sensors make them ideal for detecting low concentrations of fluoride, which is crucial for monitoring drinking water quality and ensuring compliance with health standards [18,19]. However, challenges such as ensuring adequate water solubility and minimizing interference from other anions or pH variations remain. Additionally, benzothiazole-based fluorescent probes are invaluable tools for detecting metal ions owing to their high metal binding affinity, significant fluorescence responses, and high sensitivity and selectivity [20-22].

Chapter-2: Benzothiazole based probe molecule with Amine and Amide moieties

Probe molecule	Nature of fluoride salt	Solvent of study	Types of sensors	Reference
 <p style="text-align: center;">C2-1</p>	F ⁻ as TBA salt and Cu (II)	Ethanol-Water mixture	Chromogenic and fluorometric	[42]
 <p style="text-align: center;">C2-2</p>	F ⁻ as TBA salt	DMSO, PBS	Fluorometric	[43]
 <p style="text-align: center;">C2-3</p>	F ⁻ as sodium salt	Methanol and PBS	Fluorometric	[44]
 <p style="text-align: center;">C2-4</p>	F ⁻ as TBA salt	THF	Fluorometric	[45]
 <p style="text-align: center;">C2-5</p>	F ⁻ as TBA salt	DMSO, CH ₃ CN	Chromogenic and fluorometric	[46]

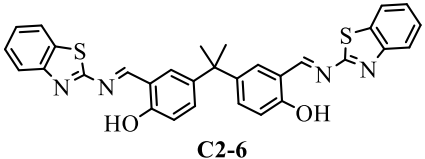
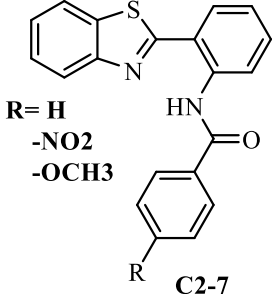
Probe molecule	Nature of fluoride salt	Solvent of study	Types of sensors	Reference
 <p style="text-align: center;">C2-6</p>	F ⁻ as TBA salt	CH ₃ CN	Chromogenic and fluorometric	[47]
 <p style="text-align: center;">C2-7</p> <p>R = H -NO₂ -OCH₃</p>	F ⁻ as TBA salt	DMSO	Chromogenic	[18]

Table 2.1: Literature report of some Benzothiazole based molecules for fluoride sensing.

Despite the number of Benzothiazole compounds found in the literature for anion sensing, most of them function efficiently only in organic mediums with anions taken as their tetraalkylammonium salts [18, 23-25]. However, it is found that the sensitivity of the probe molecule diminishes with inorganic fluoride like NaF and aqueous medium. At this point, it is envisaged that designing a Benzothiazole based probe that possesses separate anion as well as cation binding sites may offer a potential solution to this difficulty. It is anticipated that the fascinating coordination and redox chemistry of the metal ion would be worthwhile in the development of a colorimetric anion sensor for aqueous environments.

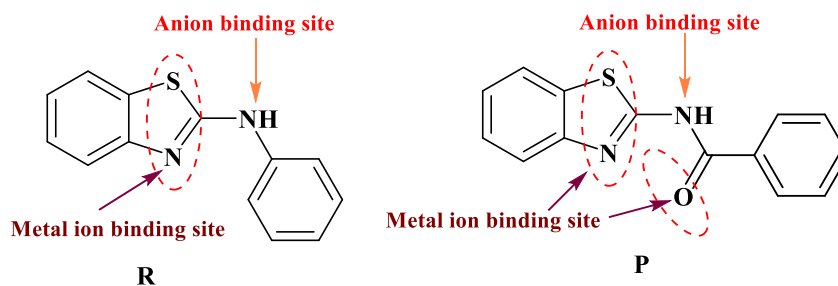


Figure 2. 1: Structure of probe molecules R & P.

In this chapter, we reported the fluoride binding affinity of two Benzothiazole based probes (**R** & **P**) (Figure 2.1) having structural features such as amine and amide -NH as an anion binding unit, along with the imine nitrogen as a metal coordinating unit. It is presumed that the insertion of a C=O group into the system would increase the anion recognition affinity of the probe by increasing the acidity of the -NH group and consequently provide good optical response.

2.2. Objective of the study

The objective of the study reported in this chapter are:

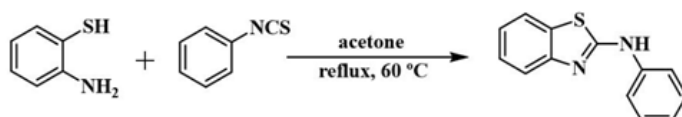
- Demonstration of the fluoride sensing affinity of the probe molecule (**R&P**) in aqueous medium by following a strategy based on hypothesis 1.
- Validation of the strategy with UV-Visible spectroscopy and electrochemical techniques like cyclic voltammogram and differential pulse voltammetry.
- Study of the efficiency of the methodology with some real-life samples.

2.3. Results and discussion

2.3.1 Synthesis and Characterization

The synthesis of the receptor is achieved by following scheme 2.1 and 2.2.

Synthesis of probe molecule **R**:

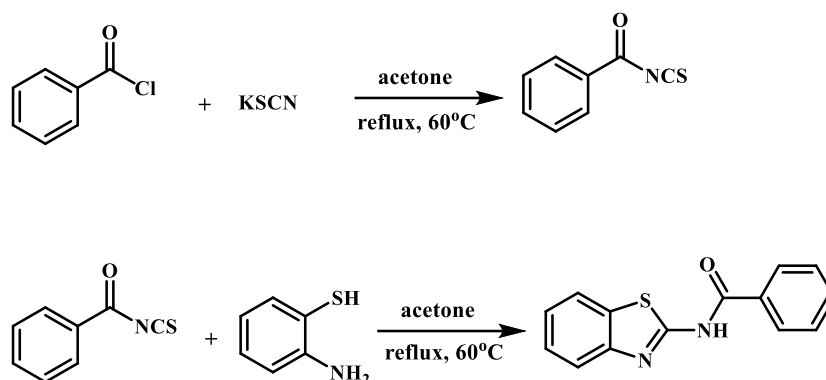


Scheme 2.1: Synthesis of **R** (*N*-phenylbenzo[*d*]thiazol-2-amine).

115 mg (0.925 mmol) of 2-aminothiophenol and 125 mg (0.925 mmol) phenyl isothiocyanate were dissolved in acetone. The mixture was then refluxed for 72h. Thereafter, the acetone was removed by distillation. The product obtained was then washed with ice-cold water. The crude product was recrystallized from ethanol.

Appearance: Brownish white, Yield: 60 %, FTIR (cm⁻¹): $\nu(\text{NH}) = 3210$, $\nu(\text{C}=\text{N}) = 1700$ and $\nu(\text{C}-\text{N}) = 1345$. ¹H NMR (400 MHz, CDCl₃, δ in ppm) δ 8.07 (s, 1H), 7.65 (m, $J = 8.4$, 1.2 Hz, 2H), 7.56 – 7.50 (m, 2H), 7.47 – 7.40 (m, 2H), 7.37 (m, $J = 8.2$, 7.3, 1.3 Hz, 1H), 7.19 (m, $J = 7.5$, 1.2 Hz, 2H). ¹³C NMR (101 MHz, CDCl₃, in ppm) δ 132.07, 129.06, 128.66, 127.92 (d, $J = 14.0$ Hz), 127.36, 126.23, 124.03, 121.44

Synthesis of probe molecule **P**:



Scheme 2.2: Synthesis of **P** (*N*-(benzo[*d*]thiazol-2-yl) benzamide)

125 mg (0.93 mmol) of Potassium thiocyanate was dissolved in acetone. To this solution, 110 μ L (0.93 mmol) of Benzoyl chloride was added slowly with constant stirring. The mixture was then refluxed for 15 min, cooled, and then filtered. To the filtrate, 115 mg (0.925 mmol) of 2-aminothiophenol in acetone solution was added slowly with continuous stirring. The mixture was then refluxed for 72 h and allowed to cool. The mixture was then poured to a beaker containing crushed ice with continuous stirring and the product was solidified. The product was filtered and subsequently recrystallized from ethanol.

Appearance: Pale brownish, Yield: 77%, FTIR (cm^{-1}): $\nu(\text{NH}) = 3395$, $\nu(\text{C}=\text{O}) = 1698$ and $\nu(\text{C}-\text{S}) = 700$. ^1H NMR (400 MHz, CDCl_3 , in ppm) δ 8.07 (t, $J = 6.4$ Hz, 2H), 7.907.84 (m, 3H), 7.52 – 7.47 (m, 4H), 7.37 – 7.32 (m, 2H), 6.17 (s, 1H). ^{13}C NMR (101 MHz, CDCl_3 , in ppm) δ 164.02, 151.60, 139.76, 130.12, 129.57, 126.17, 124.27, 122.53, 120.84, 119.96, 119.62.

The probe molecules were also characterized by single crystal X-ray diffraction analysis (appendix A2.2, table A.2.1). The crystal structure of compound **R** revealed the formation of a dimeric motif facilitated by $R_2^2(8)$ N–H...N hydrogen bonding interactions. Similarly, compound **P** demonstrated an analogous N–H...N hydrogen bonding pattern between the secondary amine N–H and the thiazole nitrogen, further reinforced by two C–H... π interactions (Figure 2.2). It was observed that other potential hydrogen bond acceptor sites, namely the carbonyl group and the sulphur atom of the thiazole unit, did not participate in the hydrogen bonding interactions.

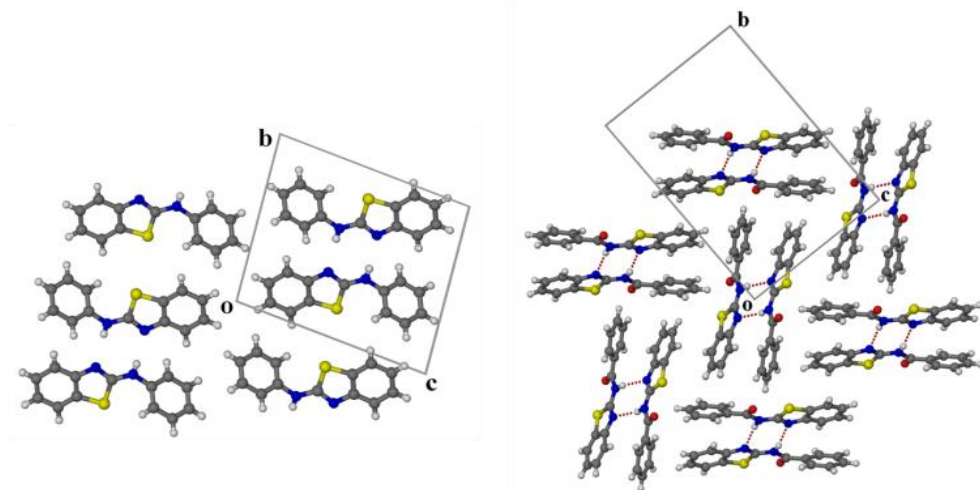


Figure 2.2: Packing diagram of left: **R** and right: **P** .

2.3.2. Anion recognition studies in organic medium

The anion binding affinity of probe molecules **R** and **P** was initially analysed using UV–Vis spectroscopy in DMSO medium. Tetrabutylammonium salt solution of various anions (F^- , Cl^- , Br^- , I^- , ClO_4^- , HSO_4^- , $H_2PO_4^-$, AcO^-) in DMSO were added to **R** and **P** solutions (6×10^{-5} M) in DMSO and the resultant colorimetric changes were monitored. The colour of **R** in DMSO solution changed from colourless to pale yellow upon addition of F^- and a very weak broad peak appeared in the region 320–360 nm in the UV-Vis spectra. Conversely, **P** exhibited a sharp peak at 360 nm upon addition of F^- and CH_3COO^- , resulting in a noticeable colour change from colourless to yellow. No appreciable colour change was observed when Cl^- , Br^- , I^- , ClO_4^- , HSO_4^- and $H_2PO_4^-$ were added to the **R** and **P** solutions in DMSO. This observation revealed that both compounds can selectively recognize fluoride ions in DMSO, with **P** showing minor interference from acetate ions (Figure 2.3). To better understand the recognition event, a UV–Vis titration experiment was conducted. For **R**, the absorbance of the peak at 281 nm decreases and the new broad absorption band's (320–360 nm) intensity enhanced upon the increase of the fluoride concentration. Similarly, the solution of **P** showed a decrease in the intensity of the peak at 305 nm, with a concomitant evolution of the peak at 360 nm upon sequential addition of fluoride, maintaining an isosbestic point at 327 nm. Job's plot showed plateau at 0.5 for both **R** and **P**, confirming the 1:1 stoichiometry for the interaction with fluoride (Figure 2.4, c-d).

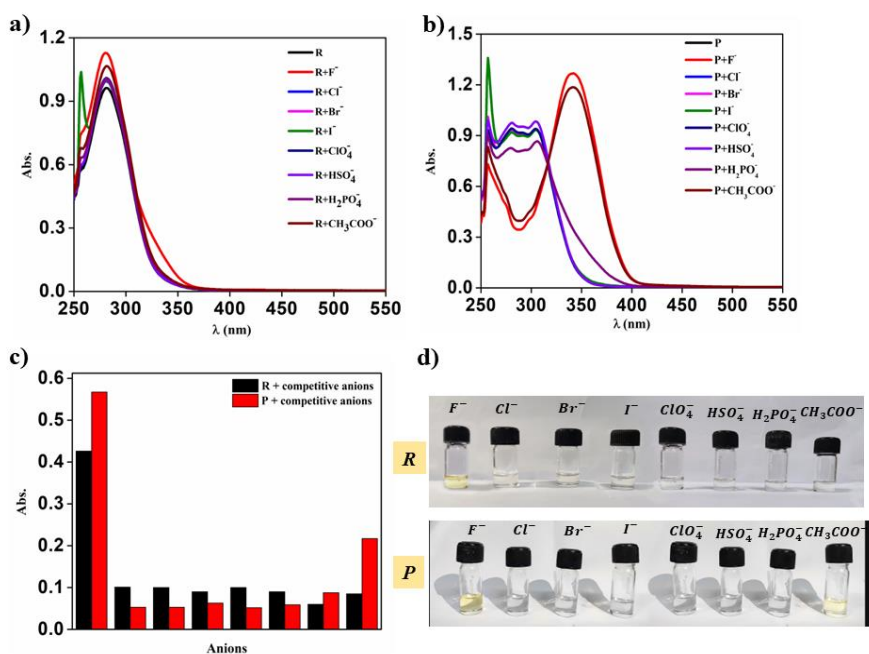


Figure 2.3: (a) UV-Vis spectra of **R** in DMSO (6×10^{-5} M) upon addition of different anions in DMSO; (b) UV-Vis spectra of **P** in DMSO (6×10^{-5} M) upon addition of different anions in DMSO; (c) Bar diagram showing changes in the absorbance of **R** (black) and **P** (red) in DMSO (both 6×10^{-5} M concentration) upon addition of different anion solutions (5×10^{-2} M); (d) Colorimetric changes upon addition of anions to **R** and **P**.

The changes in the absorption spectra were more prominent in **P** due to the higher acidity of the N–H hydrogen in **P** compared to **R**. The presence of a carbonyl moiety in **P** withdraws electron density from the N–H moiety, enhancing acidity and increasing H-bond donating and deprotonation affinity. The equilibrium constants for the interaction of **R** and **P** with fluoride were calculated from the titration data using Connor's equation and the Benesi-Hildebrand method. Curve fitting was done by considering absorption at wavelengths 334 nm for **R** and 360 nm for **P**. A linear relationship between $\left(\frac{1}{A-A_0}\right)$ and the concentration of $\frac{1}{F^-}$ ($R^2 = 0.998$ for **R** and $R^2 = 0.995$ for **P**) was observed, yielding association constants of 793 M^{-1} for **R** and 4411 M^{-1} for **P** (Figure 2.4a-b). The higher equilibrium constant for **P** is attributed to the higher acidity of its NH-hydrogen. The UV–Visible experiments indicated that receptors **R** and **P** have promising affinity for fluoride salt with an organic counter ion in DMSO. However, when TBAF was added to the DMSO solutions of **R** and **P** (6×10^{-5} M) in the presence of water, it was observed that both probe

molecules lose their affinity towards the fluoride ion even in the presence of a small amount of water.

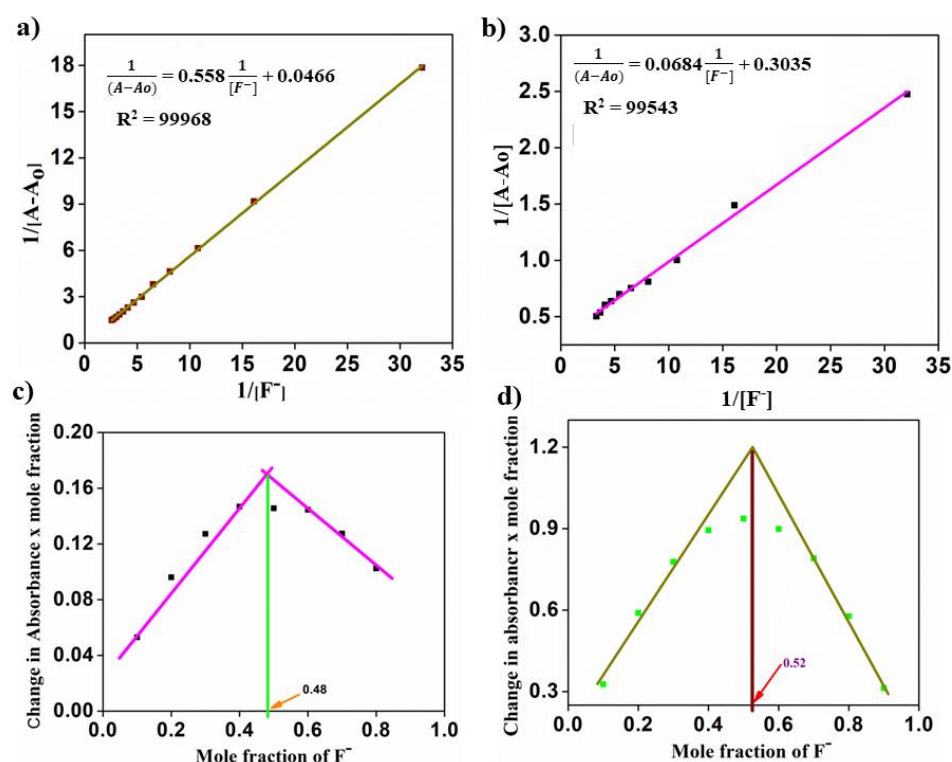


Figure 2.4: (a) UV-Vis spectra of **R** in DMSO (6×10^{-5} M) upon gradual addition of TBAF solution in DMSO; (b) UV-Vis spectra of **P** in DMSO (6×10^{-5} M) upon gradual addition of TBAF solution in DMSO; (c) Job's plot of **R** representing 1:1 stoichiometric interaction between **R** and F^- ; (d) Job's plot of **P** representing 1:1 stoichiometric interaction between **P** and F^- .

2.3.3. 1H -NMR titration study

To decipher the nature of interactions between probe molecules (**R** and **P**) and fluoride ions, the changes in the 1H NMR spectra of **R** and **P** were monitored upon gradual addition of different equivalents of fluoride ion. The 1H NMR spectra in DMSO- d_6 (23×10^{-3} M) solution showed the signal for thiazole NH protons at $\delta = 9.79$ ppm and $\delta = 12.89$ ppm for **R** and **P**, respectively. The other protons corresponding to the aromatic rings appeared in the range of 7.0–8.2 ppm. The downfield shift of the N-H proton of **P** relative to **R** might be due to the presence of the adjacent electron-withdrawing carbonyl moiety and the involvement of the N-H proton in intramolecular H-bonding. Upon addition of fluoride ion to the solution of **R**, the N-H peak at 9.79 ppm broadened, and the entire aromatic proton

region underwent an up-field shift owing to the H-bonding interaction between **R** and F^- , which increases the electron density in the phenyl and thiazole moieties (Figure 2.5). However, in the case of **P**, the N-H peak shifted up-field from 12.89 to 12.6 ppm with concomitant broadening, indicating some conformational change in **P** induced by the fluoride ion during the initiation of H-bonding interaction with the N-H moiety of **P** (Figure 2.5). The N-H peak finally disappeared upon addition of three equivalents of fluoride ion,

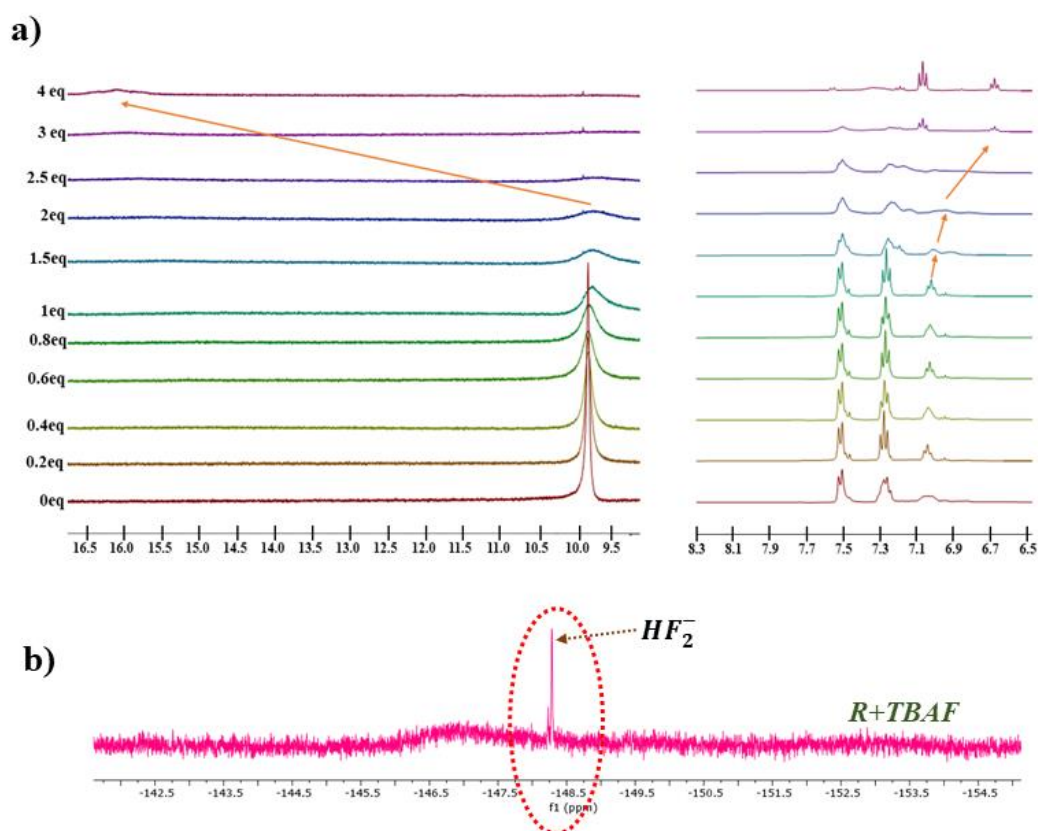


Figure 2.5: (a) Change in the 1H -NMR signals of receptor **R** in $DMSO-d_6$ upon addition of fluoride ion; (b) ^{19}F -NMR of TBAF titration to probe **R**.

and a new peak corresponding to HF_2^- appeared at 16 ppm, confirming deprotonation. The aromatic protons corresponding to the benzothiazole unit of **P** showed an up-field shift upon incremental addition of fluoride, while the protons corresponding to the benzoyl moiety remained intact (Figure 2.6). The N-H deprotonation by F^- ion enhances the electron density of the thiazole moiety due to delocalization of the excess electron density, resulting in an up-field shift of the aromatic proton signals. The 1H -NMR titration study revealed

that both molecules interact with fluoride ions through H-bonding followed by Brønsted acid-base deprotonation equilibrium leading to the abstraction of -NH proton by F⁻ ion.

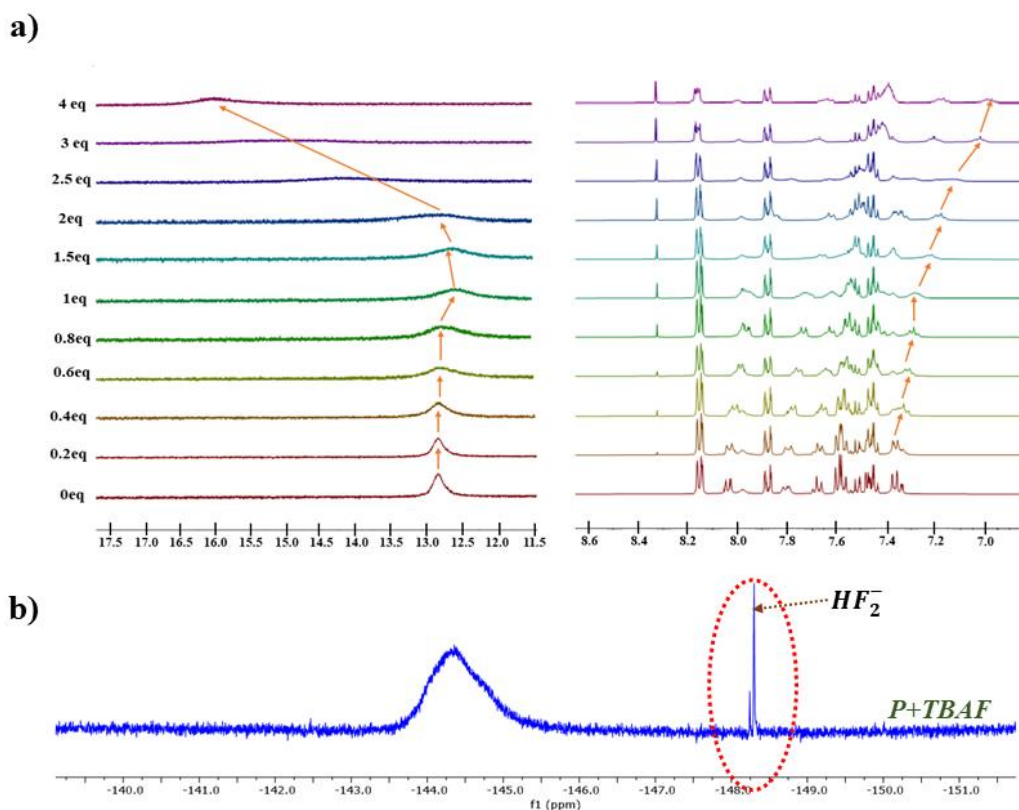


Figure 2.6: (a) Change in the ¹H-NMR signals of receptor **P** in DMSO-*d*₆ upon addition of fluoride ion; (b) ¹⁹F-NMR of TBAF titration to probe **P**.

2.3.4. Fluoride recognition study of **R** and **P** in aqueous medium

2.3.4.1. UV-Vis spectroscopy study

Although compounds **R** and **P** exhibit notable sensitivity to fluoride ions in organic mediums, their affinity decreases even in the presence of small amounts of water. This is due to the instability of the conjugate base of the probe molecules and the lower basicity of fluoride ions in aqueous medium. It is hypothesized that stabilizing the conjugate base of the sensor probe molecule through in-situ transition metal complexation could favour the deprotonation equilibrium in water, thereby aiding in the recognition of fluoride ions in aqueous medium. To test this hypothesis, the stability of the conjugate base of the probe molecules was assessed in the presence of metal ions to improve the colorimetric response and facilitate the deprotonation equilibrium in aqueous medium. Initially, the affinity of

compounds **R** and **P** towards various metal salts (NaCl, VCl₃, MnCl₂, CoCl₂, NiCl₂·6H₂O, CuCl₂·2H₂O, ZnCl₂, SrCl₂, BaCl₂, MgCl₂, FeSO₄) was tested. Chloride and sulphate salts of metal ions were selected for this investigation because the probe molecules **R** and **P** showed no affinity for these anions. It was observed that both probe molecules did not exhibit any affinity towards the tested metal ions (Figure 2.7a-b). Subsequently the affinity of the deprotonated probe, i.e., **R**⁻ and **P**⁻ towards the metal ions were studied. The addition of an aqueous solution of Cu²⁺ ions to the **R**·F⁻ solution changed the colour of the solution into dark yellow (Figure 2.7e). The absorption spectra of **R**·F⁻ solution displayed a bathochromic shift of approximately 40 nm for the peak at 287 nm upon addition of aqueous Cu²⁺ ions, along with the evolution of a broad peak at 350-400 nm (Figure 2.7c). In the case of the **P**·F⁻ solution, the solution's colour remained unchanged upon the addition of Ni²⁺, Cu²⁺, and Na⁺ ions in water and the peak 360 nm remained intact. The addition of aqueous solutions of other metal ions led to the disappearance of the absorption peak at 360 nm, which is characteristic of the interaction between **P** and fluoride ions. This observation indicates the stabilization of **P**⁻ by Ni²⁺, Cu²⁺, and Na⁺ ions, whereas other metal ions could not stabilize **P**⁻, shifting the deprotonation equilibrium towards the left in an aqueous medium (Figures 2.8). Gradual addition of aqueous NaF solution to **P** in the presence of Ni²⁺ or Cu²⁺ ions resulted in a gradual increase in the absorption peak intensity. Interestingly, the addition of aqueous NaF solution to **P** in DMSO, in the absence of any metal ions, also resulted in a gradual increase in absorbance at approximately 360 nm (Figures 2.8d). This is likely due to the higher stability of the sodium salt of deprotonated **P** in the aqueous DMSO medium. Although this observation is promising, detecting fluoride ion response required a higher concentration of fluoride, which is not practical for our purposes as our objective is to make sensor capable to detect fluoride in drinking water upto 1 ppm level. However, the change in absorbance of **P** with increasing fluoride ion concentration in the presence of Ni(II) ions was found to be more consistent and precise. Therefore, the probe molecule **P** combined with Ni(II) ions is considered as the more suitable combination for the fluoride sensing methodology (Figure 2.8b). The limit of detection (LOD) value was calculated using the formula $3.3 \times SD/m$, where SD is the standard deviation of the blank and m is the slope of the calibration plot in the presence of metal ions [26]. The calculated LOD for the probe molecule **P** in the presence of Ni(II) salt was found to be 0.5 ppm. This study clearly indicates that benzothiazole-based organic probe molecules can be used for sensing fluoride ions in aqueous mediums in the presence of transition metal ions (Cu²⁺ and Ni²⁺).

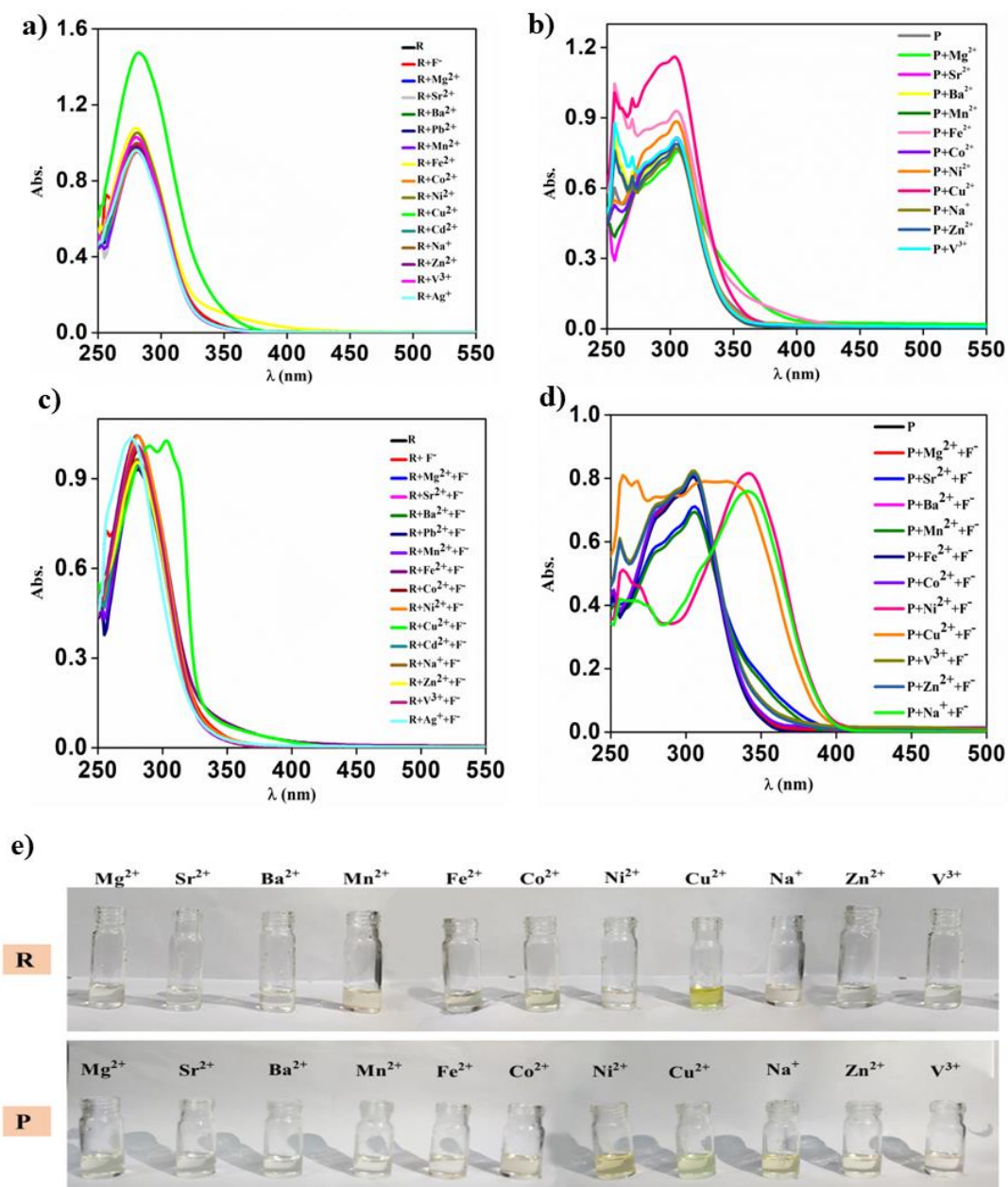


Figure 2.7: UV-Vis absorbance of the probe molecules [6×10^{-5} M] in DMSO solution upon addition of different metal salts [10×10^{-3} M] (NaCl, MgSO₄, VCl₃, MnCl₂, FeSO₄, CoCl₂, NiCl₂.6H₂O, CuCl₂.2H₂O, ZnCl₂, SrCl₂, BaSO₄,) as aqueous solution (a) **R** in absence of F⁻ ion; (b) **P** absence of F⁻ ion; (c) **R** in presence of F⁻ ion; (d) **P** in presence of F⁻ ion; (e) Images of the colorimetric changes upon the above addition.

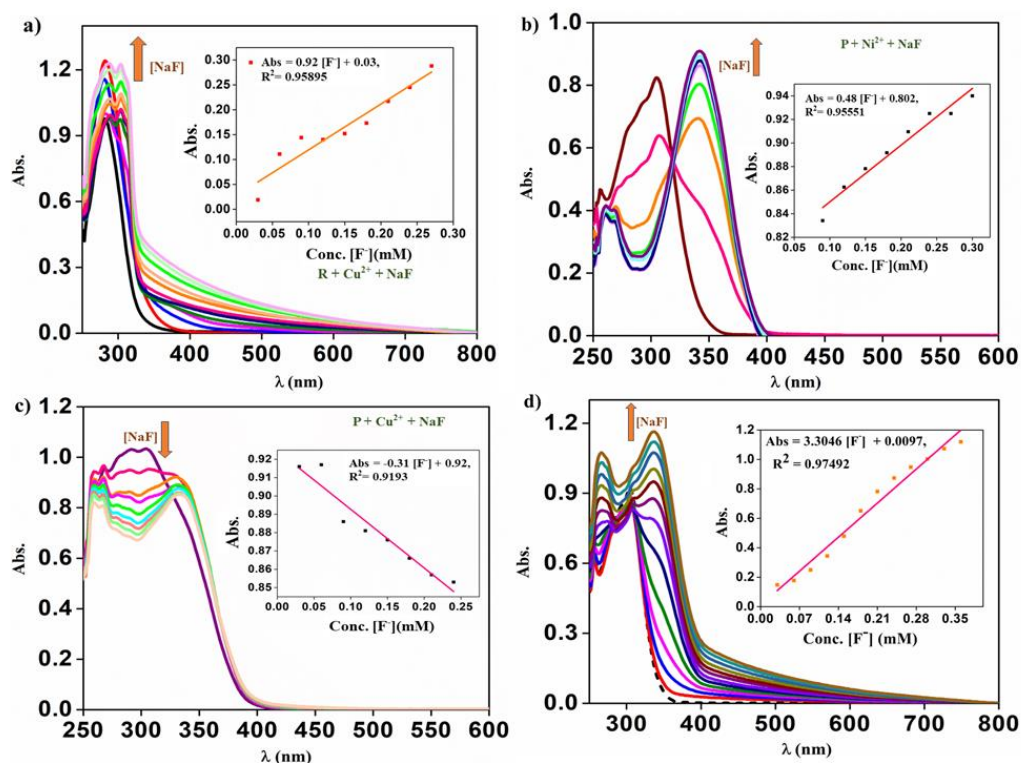


Figure 2.8: UV-Vis spectra of (a) **R** [6×10^{-5} M] with varying NaF [1×10^{-3} M] concentration in presence of Cu^{2+} cation [1×10^{-3} M]; (b) **P** [6×10^{-5} M] with varying NaF [10×10^{-3} M] concentration in presence of Cu^{2+} cation [1×10^{-3} M]; (c) **P** with varying NaF [1×10^{-3} M] concentration in presence of Ni^{2+} cation [1×10^{-3} M]; (d) **P** [6×10^{-5} M] with varying NaF [1×10^{-3} M] concentration in absence of any metal ion.

2.3.4.2. Electrochemical study

To further validate our experiment, an electrochemical study was conducted. The electrochemical behaviour of **R** and **P** was analysed using cyclic voltammetry and differential pulse voltammetry techniques upon the stepwise addition of fluoride in presence of the metal ion (Cu^{2+} or Ni^{2+}). Both the probe molecules **R** and **P** exhibited reduction peaks at -1.258 V and -1.324 V, respectively. However, the addition of F^- ions resulted in a quasi-reversible redox system with ($E_{pc} = -0.939$ V, $E_{pa} = 0.294$ V, $\Delta E = 1.233$ V) for **R** and ($E_{pc} = -1.02$ V, $E_{pa} = 1.096$ V, $\Delta E = 1.44$ V) for **P** (Figure 2.9a,c). Subsequently, the addition of aqueous CuCl_2 to the **R**· F^- solution caused the anodic peak to shift towards a higher potential ($E_{pa} = 0.879$ V) and the appearance of peaks corresponding to the $\text{Cu}^{2+}/\text{Cu}^+$ redox couple (Figure 2.9b). Similarly, the addition of Cu(II) solution to the mixture of **P** and F^- resulted in the anodic peak of **P** shifting to a lower

potential (Epa = 0.456 V) along with the emergence of the peak corresponding to the Cu(II) centre (Figure 2.9d) [27,28]. This observation indicates the in-situ complexation of the deprotonated probe

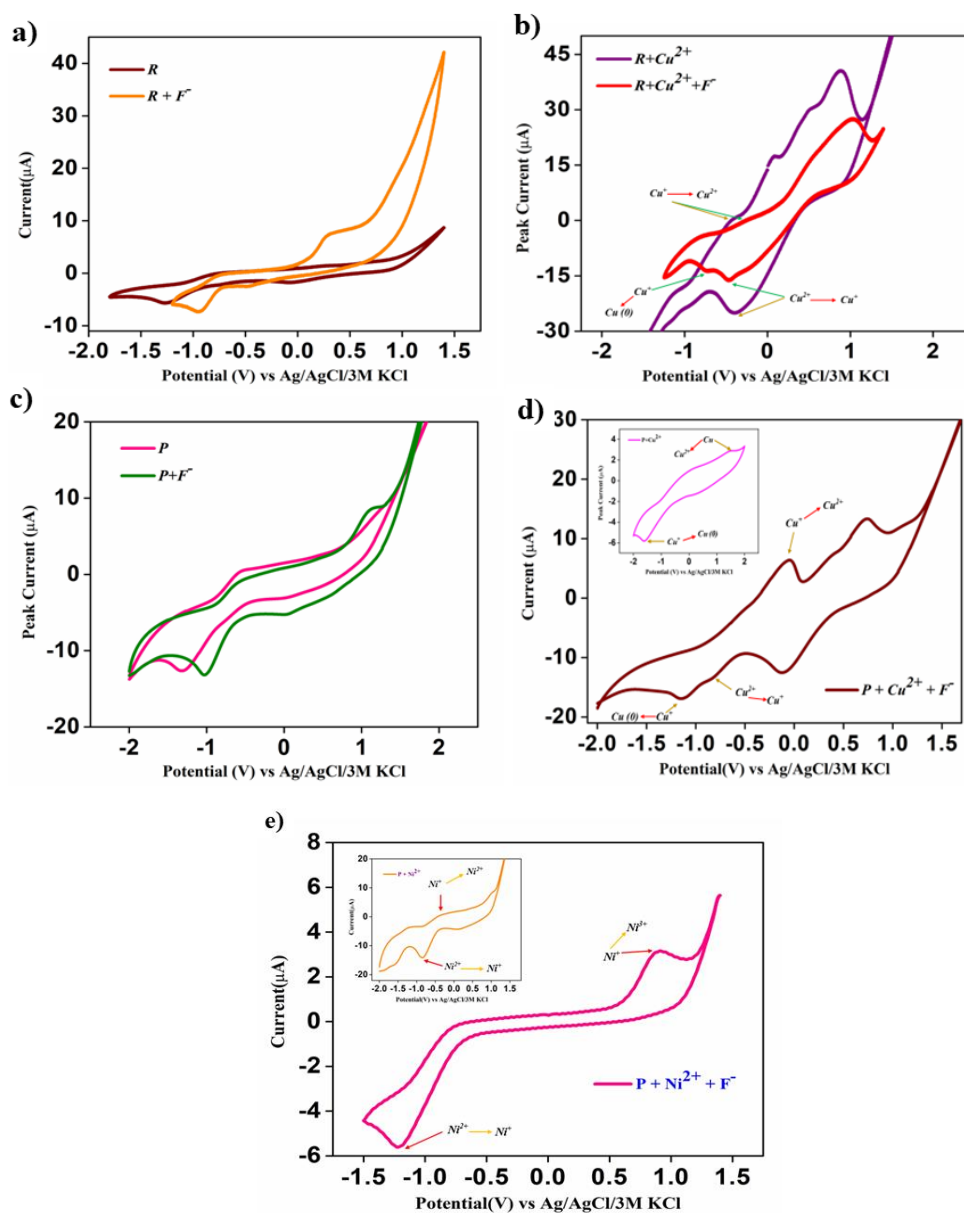


Figure 2.9. Cyclic voltammogram recorded in 0.01 M TBAP (DMSO) interaction of (a) 50mV/s -100mV/s in case of **R**; (b) Cyclic voltammogram of receptor **R** [6×10^{-5} M] in presence of F⁻ [1×10^{-3} M] anion and Cu²⁺ [1×10^{-3} M] ion; (c) 50mV/s -90mV/s in case of **P** [6×10^{-5} M] with F⁻ [1×10^{-3} M]; (d) Cycle voltammogram of receptor **P** [6×10^{-5} M] in presence of F⁻ [1×10^{-3} M] anion and Cu²⁺ [1×10^{-3} M] ion; inset: CV of **P** and Ni²⁺ in absence of F⁻; (e) Cycle voltammogram of receptor **P** [6×10^{-5} M] in presence of F⁻ [1×10^{-3} M] and Ni²⁺ [1×10^{-3} M] ion; inset: CV of **P** and Ni²⁺ in absence of F⁻.

molecule with the Cu(II) ion. Furthermore, the addition of NiCl₂ to the **P**·F⁻ mixture resulted in a ligand-centred quasi-reversible peak at E_{pc} = -1.204 V and E_{pa} = 0.898 V, with a peak-to-peak separation of ΔE = 2.102 V, along with the peak corresponding to the Ni(II)/Ni(I) redox couple (Figure 2.9e) [29,30]. To investigate the kinetics of the electrochemical behaviour on a glassy carbon electrode (GCE), the effect of scan rate on electrochemical signals was recorded for samples containing all three components (**R** or **P**, F⁻, and CuCl₂ or NiCl₂) at scan rates of 40, 60, 70, 80, and 90 mV·s⁻¹. It was observed that the anodic peak shifted slightly to a more positive potential, and the current increased linearly with increasing scan rate. The corresponding Randles-Sevick plot, i.e., the plot of peak current (I_p) vs. the square root of scan rate (v^{1/2}), revealed diffusion-cum-adsorption controlled kinetic processes for all three systems (Figure 2.10) [31,32].

Differential pulse voltammetry (DPV) of **R** and **P** solutions in DMSO in the presence of aqueous CuCl₂ salt, upon gradual addition of F⁻, was monitored by sweeping the potential from 0.2 to 0.8 V [33]. For the DPV experiment, the oxidation peaks of the deprotonated

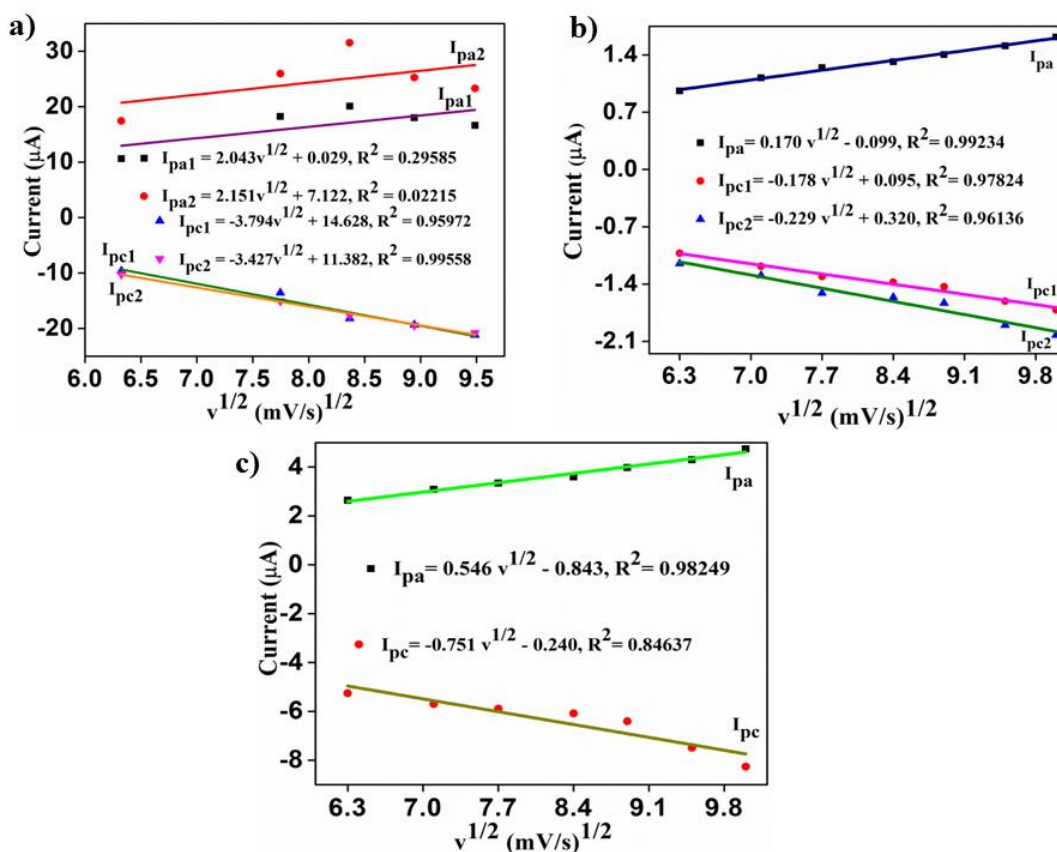


Figure 2.10: (a) RS plot for **R**·F⁻ in presence Cu²⁺ ion; (b) RS plot for **P**·F⁻ in presence Cu²⁺ ion; (c) RS plot for **P**·F⁻ in presence Ni²⁺ ion.

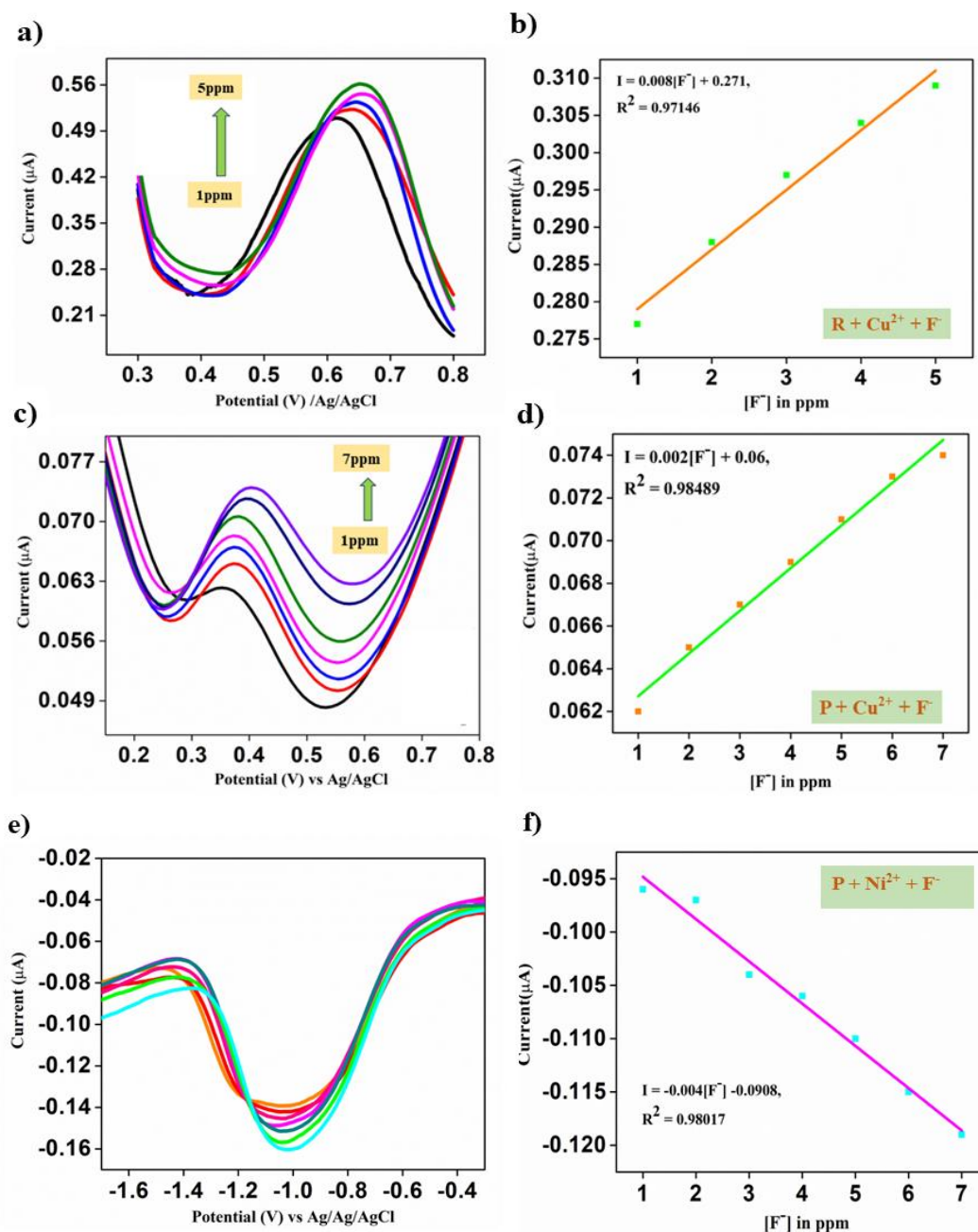


Figure 2.11: (a) Change in the DPV plots of **R** upon gradual addition of fluoride in presence of Cu (II) salt; (b) The calibration curve for the titration shown in (a); (c) changes in the DPV plots of **P** upon gradual addition of fluoride in presence of Cu (II) salt; (d) the calibration curve for the titration shown in (c); (e) change in the DPV plots of **P** upon gradual addition of fluoride in presence of Ni(II) salt; (f) the calibration curve for the titration shown in d.

probe molecules were considered. In both cases, the peak potential and the height of the anodic peak shifted slightly positive as the concentration of F^- ions increased. The change in peak height against the concentration of F^- showed good linear fitting in both cases with appreciable RMSD values. Similarly, in the DPV study of **P** in the presence of $NiCl_2$, the reduction peak of **P** was monitored against the concentration of F^- in the potential range of -1.6 to -0.4 V. The DPV plot revealed a linear increase in the current of the cathodic peak with increasing concentration of fluoride. The DPV experiment suggested that probe molecules **R** and **P** could be used as electrochemical sensor probes for detecting F^- ions in water medium in the presence of Cu^{2+} and Ni^{2+} ions (Figure 2.11). The LOD values calculated for the detection of aqueous F^- ions were 1 ppm for **R** in the presence of Cu^{2+} , whereas **P** has LOD values of 0.57 ppm and 1.65 ppm in the presence of Ni^{2+} and Cu^{2+} ions, respectively.

2.3.4.3. Investigation of the sensing mechanism

To get insight into the structure of the in-situ metal complex formed during the sensing process, the reaction mixture was precipitated out and analysed with FTIR spectroscopy. The in-situ metal complexation is confirmed by the presence of IR peaks characteristic of M-N and M-O vibrations in the FT-IR spectra of the isolated complexes (Figure 2.12) [34].

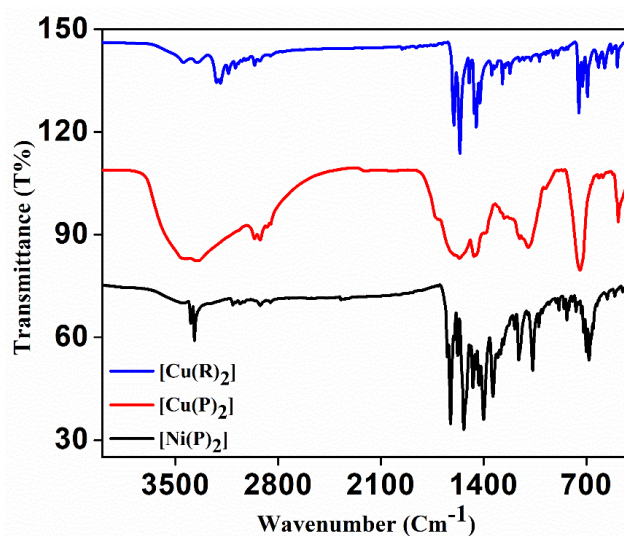


Figure 2.12: Experimental IR spectra of $[Ni(P)_2]$ complex, $[Cu(P)_2]$ complex and $[Cu(R)_2]$ complex.

To decipher the oxidation state of the metal ion and understand the mechanism of the recognition event, EPR analysis of the reaction mixture was performed in frozen aqueous

dimethyl sulphoxide solution. The X-band (9.44 GHz) EPR spectra of **R** and **P**, upon stepwise addition of $\text{CuCl}_2 \cdot 2\text{H}_2\text{O}$ (aq) and F^- (aq), unequivocally illustrate the change in the coordination environment of the Cu(II) species (Figure 2.13) [35-36]. The shape and calculated g -values of the EPR spectra of the mixture of **R** and CuCl_2 solution indicate an elongated octahedral environment around the Cu(II) centre, where the ground state is a

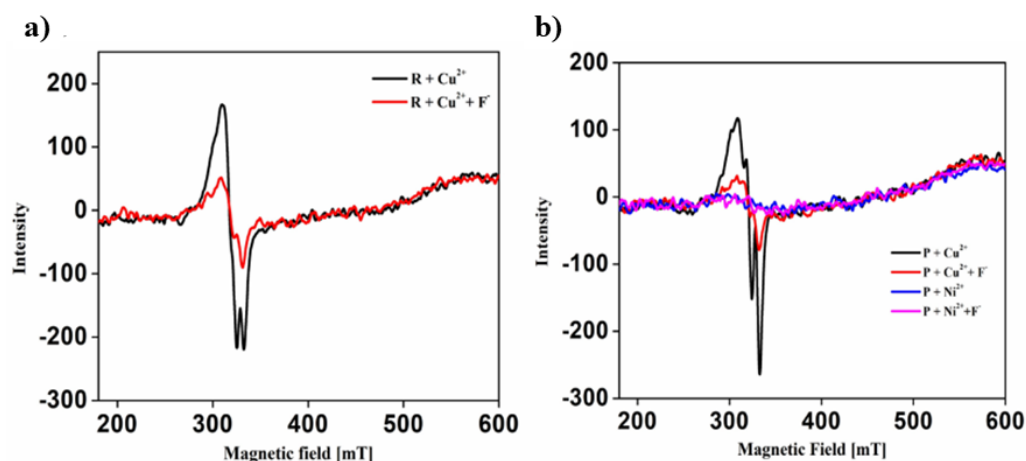


Figure 2.13: EPR spectra (Freq:9441.38 MHz, 100 K, DMSO) (a) black: addition of CuCl_2 (aq.) to the **R** solution; red: addition of CuCl_2 (aq) to the **R** solution followed by F^- in DMSO; (b) black: addition of CuCl_2 (aq.) to the **P** solution; red: addition of CuCl_2 (aq) to the **P** solution followed by F^- in DMSO; blue: addition of NiCl_2 (aq.) to the **P** solution; pink: addition of NiCl_2 (aq) to the **P** solution followed by F^- in DMSO.

combination of d_{z^2} and $d_{x^2-y^2}$ orbitals (Table 2.2) [37]. Upon the addition of F^- ions, the g -value increases slightly with a concomitant decrease in signal intensity. This observation suggests a lowering of the concentration of paramagnetic species in the sample, indicating a dynamic interconversion of some Cu(II) species to the Cu(I) complex in the reducing environment generated by the addition of aqueous F^- ions in DMSO. The plausible mechanism involved in the sensing process is depicted in figure 2.14. A similar finding was also observed with **P**. Furthermore, the EPR spectra of the solution in the presence of Ni^{2+} and F^- did not show any peaks, confirming the diamagnetic nature of the Ni(II) complexation.

Complex	g_x	g_y	g_z
$\mathbf{R} + \text{Cu}^{2+} (\text{aq})$	2.174	2.068	2.025
$\mathbf{R} + \text{Cu}^{2+} (\text{aq}) + \text{F}^- (\text{aq})$	2.187	2.092	2.036
$\mathbf{P} + \text{Cu}^{2+} (\text{aq})$	2.183	2.079	2.026
$\mathbf{P} + \text{Cu}^{2+} (\text{aq}) + \text{F}^- (\text{aq})$	2.190	2.092	2.029

Table 2.2: Components of g of Cu(II) metal centres in the different chemical environment.

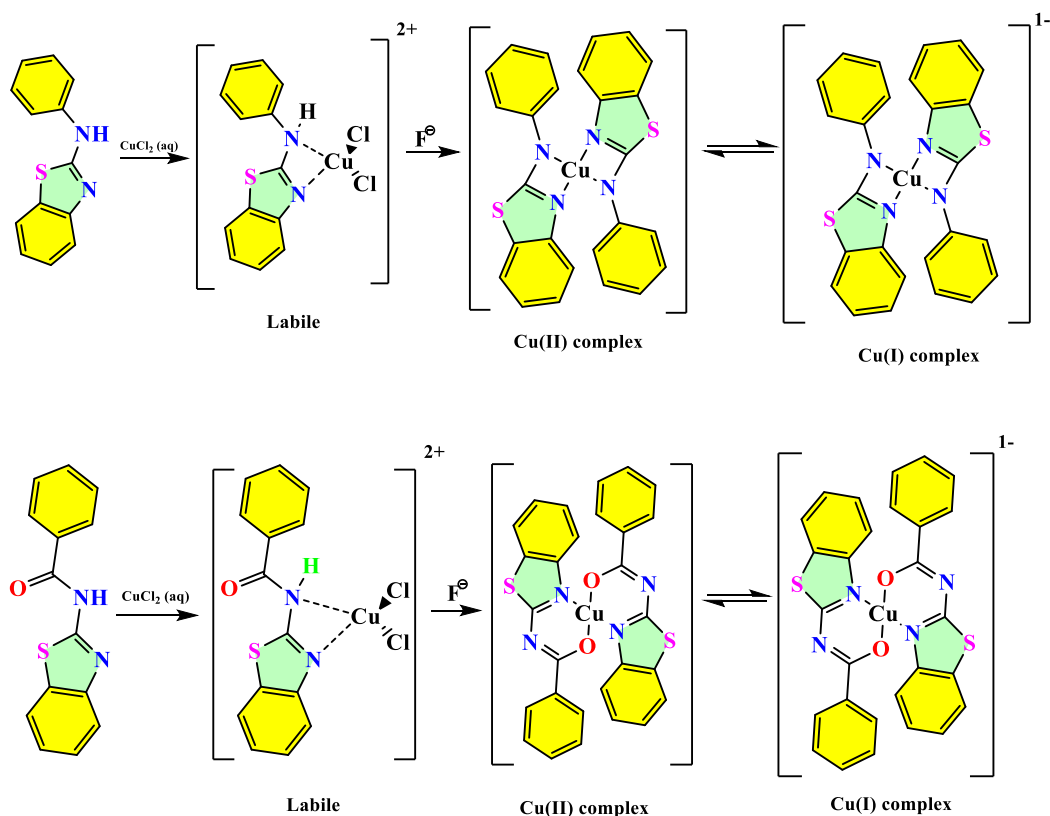


Figure 2.14: Plausible mechanism involved in the process.

2.3.4.4. DFT study

From the results of $^1\text{H-NMR}$, EPR, and FT-IR studies, it can be concluded that the recognition of fluoride ions in an aqueous medium by the probe molecules **R** and **P** occurs due to the in-situ complex formation of the deprotonated probe molecules with the respective metal ions (Ni^{2+} and Cu^{2+}). To elucidate the structure of the in-situ complex

formed during the sensing process, density functional theory (DFT), time-dependent density functional theory (TDDFT), and natural bond orbital (NBO) calculations were performed in a DMSO medium. The simulated spectra resulting from the optimized structures were further validated with experimental results such as UV-Vis and FT-IR spectroscopy data.

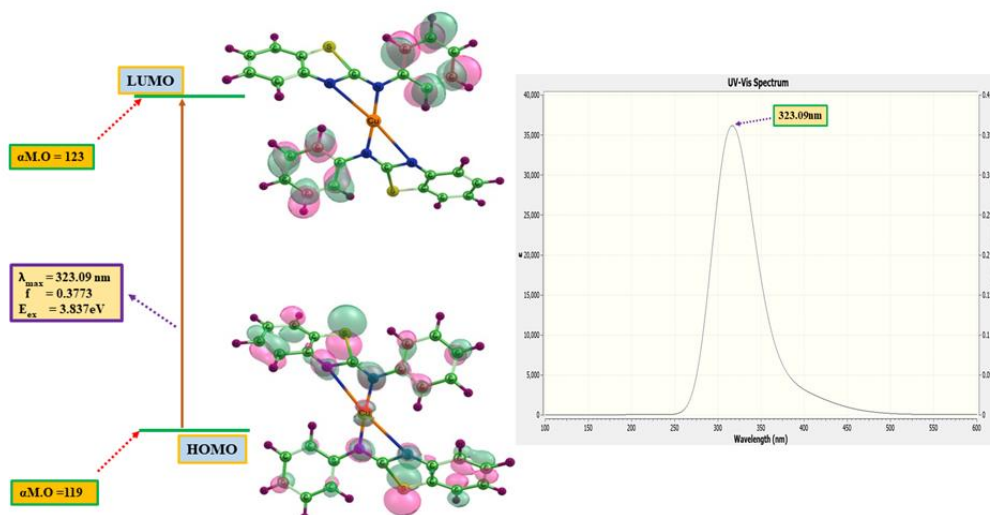


Figure 2.15: Left: Frontier molecular orbitals involved in the UV-Vis absorption of [Cu(**R**)₂]; Right: TDDFT calculated UV-Vis spectra of [Cu(**R**)₂].

For probe **R**, the [Cu(**R**)₂] complex adopts a distorted square planar structure with Cu-N coordination, where bond distances range between 1.84 – 2.10 Å. The simulated UV-Vis spectra for [Cu(**R**)₂] in DMSO solvent system closely resemble the experimental spectra, showing a peak at 323.09 nm (Figure 2.15). Similarly, for probe **P**, the [Ni(**P**)₂] complex attains a square planar configuration, which reinforces the diamagnetic behaviour of the complex, whereas the [Cu(**P**)₂] complex adopts a distorted square planar geometry like probe molecule **R** (Figure 2.16). The second-order perturbation energy value E(2) obtained from NBO calculations revealed that deprotonated **P** coordinates with the metal centre (Ni²⁺ and Cu²⁺) via the thiazole nitrogen and the carbonyl oxygen (Table 2.3). Deprotonation of the amine proton induces delocalization of the electron density between the carbonyl oxygen and the thiazole ring, creating a suitable chelating and coordinating environment for metal complexation. The predicted IR frequency values for M-N and M-O vibrations matched the experimental values, supporting the accuracy of the predicted structures (Table

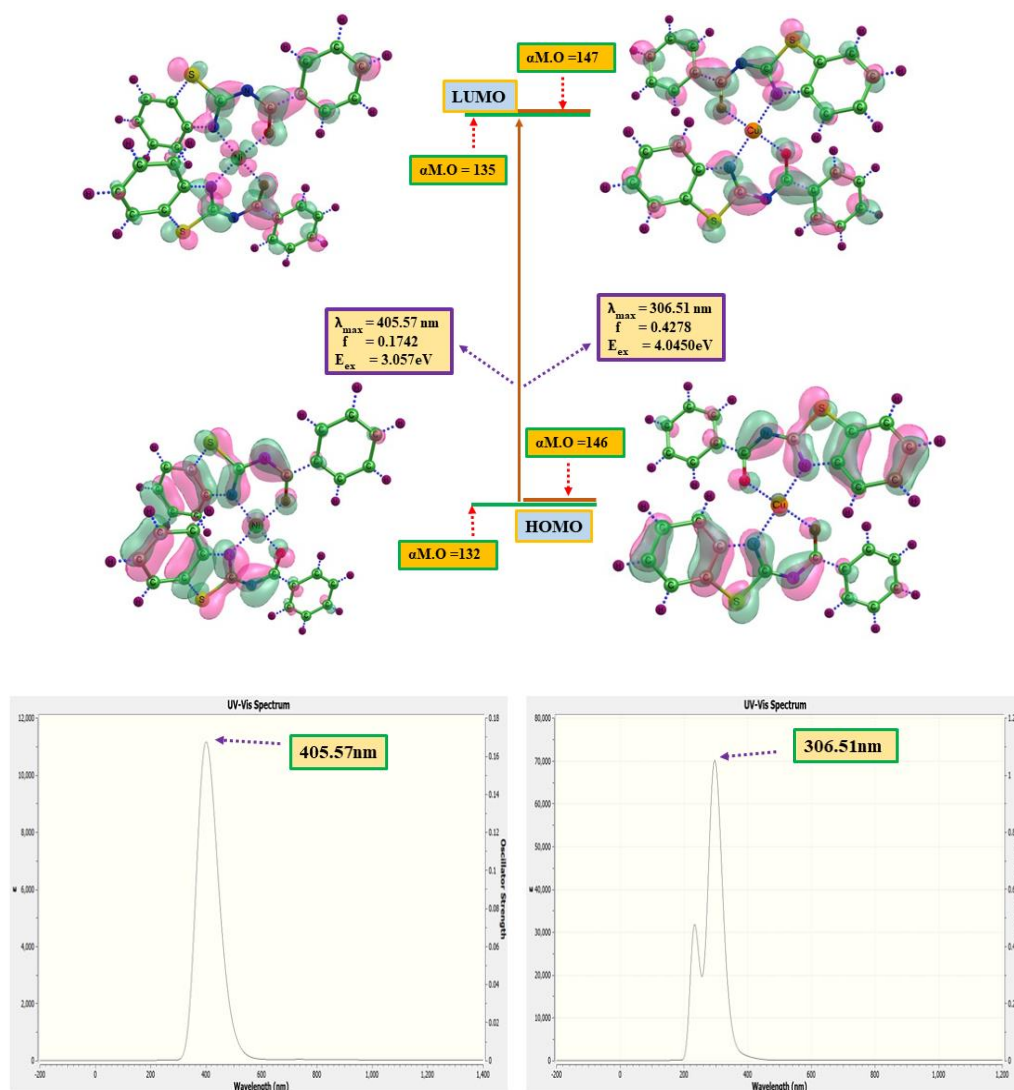


Figure 2.16: Top Left: Frontier molecular orbitals involved in the UV-Vis absorption of [Ni(P)₂]; Top Right: Frontier molecular orbitals involved in the UV-Vis absorption of [Cu(P)₂]; Bottom Left: TDDFT calculated UV-Vis graph of [Ni(P)₂]; Bottom Left: TDDFT calculated UV-Vis graph of [Cu(P)₂].

2.4) [38-40]. The simulated UV-Vis spectra of the [Ni(P)₂] complex showed a peak at 405 nm corresponding to the LMCT transition whereas the [Cu(P)₂] complex showed a weak band at 306 nm corresponding to an MLCT transition.

Complex	Donor(i)	Acceptor(j)	E ² (KJ/mol)	E _i -E _j (a.u)	F _{ij} (a.u)
[Cu(R) ₂]	LP (1) N13	LP*(6) Cu25	38.68	0.62	0.196
	BD*(1) Cu25-N39	LP*(1) Cu25	295.41	0.07	0.204
[Cu(P) ₂]	LP (1) N37	LP*(6) Cu25	26.19	0.61	0.160
	LP(1) O45	LP*(6) Cu47	702.18	0.70	0.936
[Ni(P) ₂]	LP(1) N41	LP*(5) Ni55	74.95	0.31	0.149
	LP (1) O45	LP*(5) Ni55	50.11	0.37	0.137
	LP (1) N43	LP*(5) Ni55	74.97	0.31	0.149
	LP (2) O46	LP*(5) Ni55	50.12	0.37	0.137

Table 2.3: Second order perturbation energy value E⁽²⁾ of different interactions involved in the metal complexation obtained from NBO calculation.

Sl. No.	Compound	Experimental Absorption (cm ⁻¹)	Group	Theoretical Absorption (cm ⁻¹)
1	[Cu(R) ₂]	679.14	N-Cu-N (Assymmetric stretching)	676.38
		607.95	N-Cu-O (Assymmetric stratching)	625.44
		493.58	N-Cu (stretching)	512.46
2	[Cu(P) ₂]	1564.29	N-Cu-O (twisting)	1679.22
		1455.79	N-Cu-O (scissoring)	1435.26
		732	Cu-O (stretching)	735.77
		467	N-Cu (stretching)	465.42
3	[Ni(P) ₂]	1564.29	N-Ni-O (twisting)	1679.22
		1455.79	N-Ni-O (scissoring)	1435.26
		732	N-Ni-N (stretching)	735.77

Table 2.3: Comparison of experimental and theoretical IR data.

2.3.5. Validation of the method with real life sample

As the colorimetric as well as electrochemical responds is more prominent with probe molecule **P**, we have considered the combination **P** and Ni²⁺ for real sample analysis. To validate our methodology, we initially titrated **P** in DMSO solution with various known concentrations of NaF in water solution in the presence of Ni (II) ions. With the incremental addition of NaF, a corresponding linear increase in the absorbance at 360 nm was observed with increasing amount of NaF (Figure 2.17b). Finally, the methodology was tested by

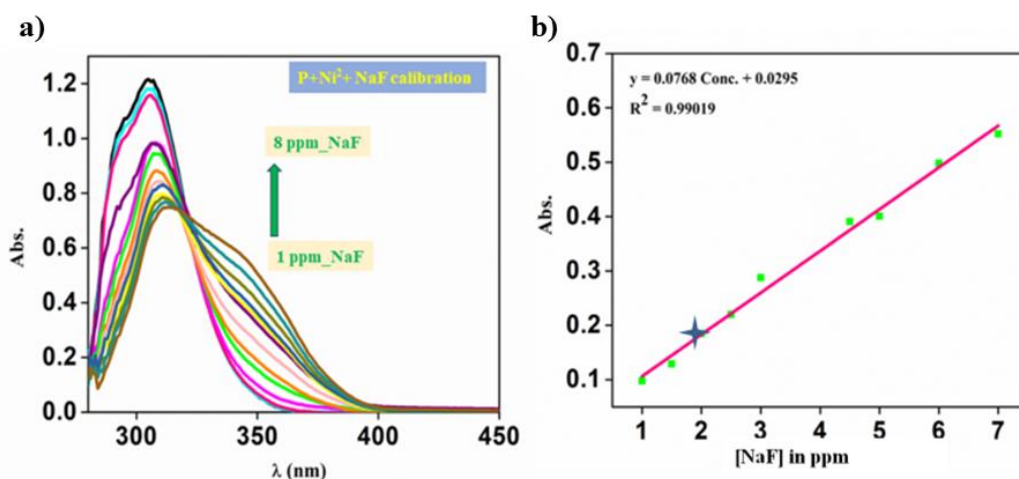


Figure 2.17: (a) Change in the UV-Vis spectra of **P** upon addition of 50 μ L of fluoride solution having different concentration in presence of Ni(II) ion; (b) Corresponding calibration plot; the blue mark indicates the absorbance of the unknown water sample.

quantifying the fluoride ion concentration in water samples collected from Dokmoka village in the Karbi Anglong district of Assam [41], India. For the analysis, a 3 mL aliquot of 6×10^{-5} M solution of **P** was placed in a cuvette, to which 50 μ L of 10×10^{-3} M NiCl₂ solution in aqueous medium was added. Subsequently, 50 μ L of the water sample was introduced to the mixture. The resultant colorimetric response was analysed using a UV-Vis spectrometer, and the absorbance at a wavelength of 360 nm was measured.

The absorbance data obtained was then compared with the calibration plot to determine the fluoride ion concentration in the water sample. The analysis revealed a fluoride ion concentration of 1.9 ppm in the water collected from Dokmoka village. This result was further corroborated with the data of fluoride ion-selective electrode, thereby confirming the accuracy and reliability of our methodology.

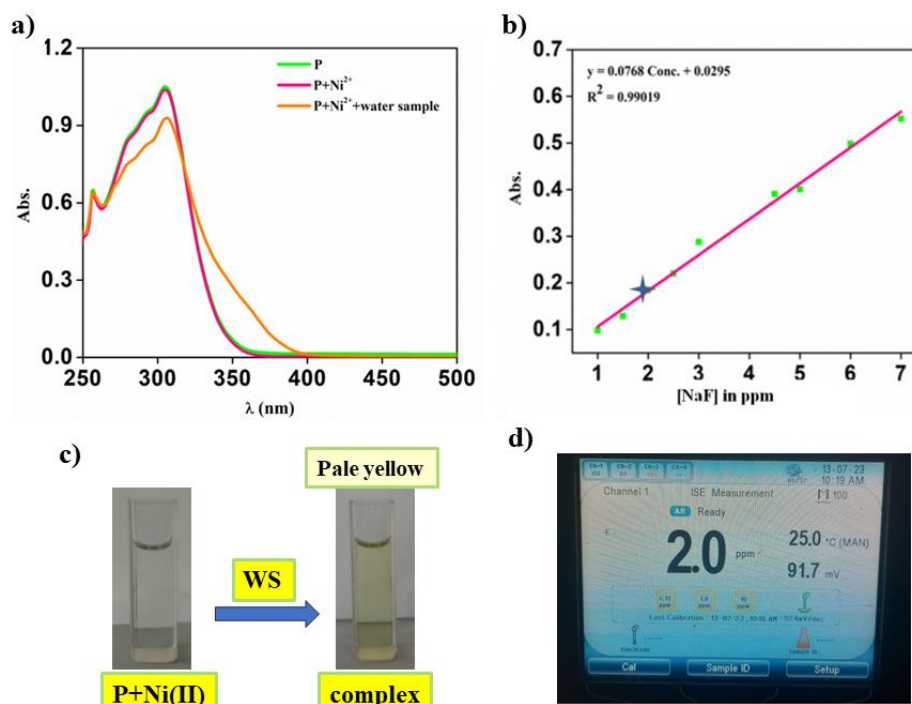


Figure 2.18: (a) Change in the UV-Vis spectra of **P** upon addition of 50 μL of water sample in presence of Ni (II) ion; (b) Calibration plot; the blue mark indicates the absorbance of the unknown water sample; (c) Image of the colorimetric changes; (d) Image of the Ion selective electrode (ISE) data indicating the concentration of water sample.

2.4. Conclusion

Although many amines and amide-based probe molecules are reported towards sensing fluoride ion in last two decades, most of them could detect fluoride ion only in the organic medium, whereas they failed to do the same in aqueous medium. In summary, we have demonstrated and validated a facile metal mediated strategy for the colorimetric determination of fluoride ion in aqueous medium with two simple amine and amide based organic probe molecules (**R** and **P**) which otherwise shows F⁻ sensitivity in organic medium only. The sustainability of the colorimetric response in aqueous medium is due to in-situ Cu²⁺ and Ni²⁺ complexation of the deprotonated probe molecules which facilitates the fluoride induced deprotonation equilibrium in water medium. The results are found to be more consistent with probe molecule **P** in presence of Ni (II) ion. The methodology was also successfully tested for the electrochemical response and demonstrated its efficiency towards fluoride ion in aqueous medium with the help of DPV technique. The methodology is further validated with groundwater samples having fluoride contamination collected

from the Karbi Anglong district of Assam (India). It is found that acetate can be a potential interfering anion in the proposed sensing methodology.

2.5. References

- [1] Liao, C., Kim, U. J., and Kannan, K. A review of environmental occurrence, fate, exposure, and toxicity of benzothiazoles. *Environmental Science & Technology*, 52(9):5007-5026, 2018.
- [2] Avagyan, R., Luongo, G., Thorsen, G., and Ostman, C. Benzothiazole, benzotriazole, and their derivatives in clothing textiles—a potential source of environmental pollutants and human exposure. *Environmental Science and Pollution Research*, 22:5842-5849, 2015.
- [3] Gill, R. K., Rawal, R. K., and Bariwal, J. Recent advances in the chemistry and biology of benzothiazoles. *Archiv der Pharmazie*, 348(3):155-178, 2015.
- [4] Chang, C., Wang, F., Qiang, J., Zhang, Z., Chen, Y., Zhang, W., and Chen, X. Benzothiazole-based fluorescent sensor for hypochlorite detection and its application for biological imaging. *Sensors and Actuators B: Chemical*, 243:22-28, 2017.
- [5] Horton, D. A., Bourne, G. T., and Smythe, M. L. The combinatorial synthesis of bicyclic privileged structures or privileged substructures. *Chemical Reviews*, 103(3):893-930, 2003.
- [6] Gao, X., Liu, J., Zuo, X., Feng, X., and Gao, Y. Recent advances in synthesis of benzothiazole compounds related to green chemistry. *Molecules*, 25(7):1675, 2020.
- [7] Dolle, R. E. Discovery of enzyme inhibitors through combinatorial chemistry. *Molecular Diversity*, 2:223-236, 1997.
- [8] Shaista, A., and Amrita, P. Benzothiazole-A magic molecule. *International Journal of Pharmaceutical Sciences and Research*, 8(12):4909-4929, 2017.
- [9] Gunawardana, G. P., Koehn, F. E., Lee, A. Y., Clardy, J., He, H. Y., and Faulkner, D. J. Pyridoacridine alkaloids from deep-water marine sponges of the family Pachastrellidae: structure revision of dercitin and related compounds and correlation with the kuanoniamines. *The Journal of Organic Chemistry*, 57(5):1523-1526, 1992.

- [10] Achson, A. *An introduction to the chemistry of heterocyclic compounds* (3rd ed.). Willy-Intersciences, India. 2009.
- [11] Shendarkar, G. R., Labhsetwar, L. B., Butle, S. R., Karki, S. S., Sharma, R. H., and Kuberkar, S. V. Synthesis and antimicrobial evaluation of some fused iminopyrimidobenzothiazole derivatives. *International Journal of Research in Pharmaceutical and Biomedical Sciences*, 2:1350-1356, 2011.
- [12] Ghoneim, K. M., El-Basil, S., Osman, A. N., Said, M. M., and Megahed, S. A. Synthesis and antimicrobial investigation of benzothiazole derivatives. *Revue Roumaine de Chimie*, 36:1355-1361, 1991.
- [13] Variya, H. H., Panchal, V., and Patel, G. R. Synthesis and spectral studies of 1,3-benzothiazole-2-thiol conjugated thiosemicarbazide as antibacterial and antifungal agents. *International Journal of Research in Advent Technology*, 7:388-392, 2019.
- [14] Yoshida, M., Hayakawa, I., Hayashi, N., Agatsuma, T., Oda, Y., Tanzawa, F., and Sugano, Y. Synthesis and biological evaluation of benzothiazole derivatives as potent antitumor agents. *Bioorganic & Medicinal Chemistry Letters*, 15(14):3328-3332, 2005.
- [15] Gupta, A., and Rawat, S. Synthesis and cyclization of benzothiazole. *Journal of Current Pharmaceutical Research*, 3:13-23, 2010.
- [16] El-Shehawy, A. A., El-Hendawy, M. M., Attia, A. M., Abdallah, A. R. I., and Abdo, N. I. Synthesis, photophysical properties, and computational studies of benzothiadiazole and/or phenothiazine-based donor/acceptor π -conjugated copolymers. *Journal of Polymer Research*, 28(7):268, 2021.
- [17] Krupka, O., and Hudhomme, P. Recent Advances in Applications of Fluorescent Perylenediimide and Perylenemonoimide Dyes in Bioimaging, Photothermal and Photodynamic Therapy. *International Journal of Molecular Sciences*, 24(7):6308, 2023.
- [18] Dhaka, G., Singh, J., and Kaur, N. Benzothiazole possessing reversible and reusable selective chemosensor for fluoride detection based on inhibition of excited state intramolecular proton transfer. *Inorganica Chimica Acta*, 450:380-385, 2016.

- [19] Borah, N., De, S., Gogoi, A., and Das, G. A series of benzothiazole-based Schiff bases for the colorimetric sensing of fluoride and acetate ions: acetate-induced turn-on fluorescence for selectivity. *New Journal of Chemistry*, 44(43), 18703-18713, 2020.
- [20] Pothulapadu, C. A. S., Jayaraj, A., Priyanka, R. N., and Sivaraman, G. Novel benzothiazole-based highly selective ratiometric fluorescent turn-on sensors for Zn²⁺ and colorimetric chemosensors for Zn²⁺, Cu²⁺, and Ni²⁺ ions. *ACS omega*, 6(38):24473-24483, 2021.
- [21] El-Nahass, M. N., Fayed, T. A., El-Daly, H. A., and Youssif, M. M. Benzothiazole azo derivatives as colorimetric probes for optical recognition of different metal ions and anions. *Applied Organometallic Chemistry*, 36(6):e6703, 2022.
- [22] Enbanathan, S., Munusamy, S., Jothi, D., Manojkumar, S., Manickam, S., and Iyer, S. K. Zinc ion detection using a benzothiazole-based highly selective fluorescence “turn-on” chemosensor and its real-time application. *RSC advances*, 12(43):27839-27845, 2022.
- [23] Chen, X., Leng, T., Wang, C., Shen, Y., and Zhu, W. A highly selective naked-eye and fluorescent probe for fluoride ion based on 1, 8-naphthalimide and benzothiazole. *Dyes and Pigments*, 141:299-305, 2017.
- [24] Hu, W., Zeng, L., Wang, Y., Liu, Z., Ye, X., and Li, C. A ratiometric two-photon fluorescent probe for fluoride ion imaging in living cells and zebrafish. *Analyst*, 141(18):5450-5455, 2016.
- [25] Du, M., Huo, B., Li, M., Shen, A., Bai, X., Lai, Y., and Yang, Y. A “Turn-On” fluorescent probe for sensitive and selective detection of fluoride ions based on aggregation-induced emission. *RSC advances*, 8(57):32497-32505, 2018.
- [26] Armbruster, D. A., and Pry, T. Limit of blank, limit of detection and limit of quantitation. *The clinical biochemist reviews*, 29(Suppl 1):S49, 2008.
- [27] Guk, D., Naumov, A., Krasnovskaya, O., Tafeenko, V., Moiseeva, A., Pergushov, V., and Beloglazkina, E. Three types of copper derivatives formed by CuCl₂ · 2H₂O interaction with (Z)-3-aryl-2-(methylthio)-5-(pyridine-2-ylmethylene)-3, 5-dihydro-4H-imidazol-4-ones. *Dalton Transactions*, 49(41):14528-14535, 2020.

- [28] Franco, E., Lopez-Torres, E., Mendiola, M., and Sevilla, M. Synthesis, spectroscopic and cyclic voltammetry studies of copper (II) complexes with open chain, cyclic and a new macrocyclic thiosemicarbazones. *Polyhedron*, 19(4):441-45, 2000.
- [29] Tang, H. M., and Fan, W. Y. Dithiolato-Bridged Nickel (II) Salicylcysteamine Complexes as Robust Proton Reduction Electrocatalysts: Cyclic Voltammetry and Computational Studies. *Inorganic Chemistry*, 60(23):17933-17941, 2021.
- [30] Soltani, B., Ghorbanpour, M., Ziegler, C. J., Ebadi-Nahari, M., and Mohammad-Rezaei, R. Nickel (II) and cobalt (II) complexes with bidentate nitrogen-sulfur donor pyrazole derivative ligands: Syntheses, characterization, X-ray structure, electrochemical studies, and antibacterial activity. *Polyhedron*, 180:114423, 2020.
- [31] Chu, T., Popov, I. A., Andrade, G. A., Maurya, S., Yang, P., Batista, E. R., and Davis, B. L. Linked picolinamide nickel complexes as redox carriers for nonaqueous flow batteries. *ChemSusChem*, 12(7):1304-1309, 2019.
- [32] Vaughn, B. A., Brown, A. M., Ahn, S. H., Robinson, J. R., and Boros, E. Is less more? Influence of the coordination geometry of Copper (II) picolinate chelate complexes on metabolic stability. *Inorganic chemistry*, 59(22), 16095-16108, 2020.
- [33] Gupta, R. K., Pandey, R., Singh, R., Srivastava, N., Maiti, B., Saha, S., and Pandey, D. S. Heteroleptic dipyrinato complexes containing 5-ferrocenyldipyrromethene and dithiocarbamates as coligands: Selective chromogenic and redox probes. *Inorganic Chemistry*, 51(16):8916-8930, 2012.
- [34] Nakamoto, K. Applications in coordination, organometallic, and bioinorganic chemistry. 1997.
- [35] Wertz, J. *Electron spin resonance: elementary theory and practical applications*. Springer Science & Business Media. 2012.
- [36] Bruzzese, P. C., Salvadori, E., Jager, S., Hartmann, M., Civalleri, B., Pöpl, A., and Chiesa, M. 17O-EPR determination of the structure and dynamics of copper single-metal sites in zeolites. *Nature Communications*, 12(1):4638, 2021.
- [37] Garribba, E., and Micera, G. The determination of the geometry of Cu (II) complexes: an EPR spectroscopy experiment. *Journal of chemical education*, 83(8):1229, 2006.

- [38] Mobili, R., and Amendola, V. Photophysics of transition metal complexes (2019–2020). 2021.
- [39] Chen, H., McMahon, J. M., Ratner, M. A., and Schatz, G. C. Classical electrodynamics coupled to quantum mechanics for calculation of molecular optical properties: a RT-TDDFT/FDTD approach. *The Journal of Physical Chemistry C*, 114(34):14384-14392, 2010.
- [40] Maschietto, F., Campetella, M., Sanz García, J., Adamo, C., and Ciofini, I. Chasing unphysical TD-DFT excited states in transition metal complexes with a simple diagnostic tool. *The Journal of Chemical Physics*, 154(20), 2021.
- [41] Hanse, A., Chabukdhara, M., Gohain Baruah, S., Boruah, H., and Gupta, S. K. Fluoride contamination in groundwater and associated health risks in Karbi Anglong District, Assam, Northeast India. *Environmental monitoring and assessment*, 191(12):782, 2019.
- [42] Peng, Y., Dong, Y. M., Dong, M., and Wang, Y. W. A selective, sensitive, colorimetric, and fluorescence probe for relay recognition of fluoride and Cu (II) ions with “off-on-off” switching in ethanol–water solution. *The Journal of Organic Chemistry*, 77(20):9072-9080, 2012.
- [43] Ke, B., Chen, W., Ni, N., Cheng, Y., Dai, C., Dinh, H., and Wang, B. A fluorescent probe for rapid aqueous fluoride detection and cell imaging. *Chemical communications*, 49(25): 2494-2496, 2013.
- [44] Zheng, Y., Duan, Y., Ji, K., Wang, R. L., and Wang, B. Tuning the reaction rates of fluoride probes for detection in aqueous solution. *RSC advances*, 6(30):25242-25245, 2016.
- [45] Du, M., Huo, B., Li, M., Shen, A., Bai, X., Lai, Y., and Yang, Y. A “Turn-On” fluorescent probe for sensitive and selective detection of fluoride ions based on aggregation-induced emission. *RSC advances*, 8(57):32497-32505, 2018.
- [46] Chen, X., Leng, T., Wang, C., Shen, Y., and Zhu, W. A highly selective naked-eye and fluorescent probe for fluoride ion based on 1, 8-naphthalimide and benzothiazole. *Dyes and Pigments*, 141:299-305, 2017.

- [47] Erdemir, S., and Kocyigit, O. Reversible “off–on” fluorescent and colorimetric sensor based benzothiazole-bisphenol A for fluoride in MeCN. *Sensors and Actuators B: Chemical*, 221:900-905, 2015.